Structure of Chlorotrifluoroethylene/Vinylidene Fluoride Random Copolymers and Homopolymers by Molecular Dynamics Simulations

Richard H. Gee,* Laurence E. Fried, and Robert C. Cook

Lawrence Livermore National Laboratory, Chemistry and Materials Science Directorate, University of California, P.O. Box 808, L-268, Livermore, California 94551

Received June 21, 2000; Revised Manuscript Received February 15, 2001

ABSTRACT: We perform molecular dynamics simulations of chlorotrifluoroethylene (CTFE)/vinylidene fluoride (VDF) copolymers over a wide range of compositions and temperatures including the volumetric glass transition. Structural features of the polymers and copolymers were characterized using pair correlation functions and wide-angle X-ray scattering (WAXS) spectra. Calculated WAXS spectra for the CTFE/VDF copolymer known as Kel-F 800 are compared with experimental results and are found to compare well. The X-ray peak associated with interchain spacing is found to shift to larger scattering angles (smaller *d* spacings) as the concentration of the CTFE comonomer decreases, suggesting a transition between CTFE and VDF homopolymer interchain packing structures, consistent with earlier experiments. The strong compositional dependence is traced to packing involving the CF_2 moiety. The calculated WAXS were further deconvoluted into atom−atom contributions in an attempt to explain the origin of the peak positions found in the WAXS. The location of the first peak in the spectra did not correspond to interchain packing distances for any of the polymer compositions except the VDF homopolymer. The effect of Coulombic interactions on polymer structure is examined. We find that the importance of Coulombic interactions is greatest for pVDF. The torsional angle distribution and the characteristic ratio show greater sensitivities to Coulombic interactions than the density and the total radial distribution function.

I. Introduction

Fluoropolymers have many interesting properties not found in their hydrocarbon analogues.[1] These properties include low surface tension and coefficient of friction, piezoelectric and pyroelectric properties, low refractive index, and high chemical and thermal stabilities. Many fluoropolymers also demonstrate an unusually high density, high chemical stability, and mechanical properties suitable for use in the manufacture of pressed powder composites.[2] An understanding of the atomistic origin of many of these properties does not currently exist.

Two of the most common halogenated polymers are poly(chlorotrifluoroethylene) (pCTFE) and poly(vinylidene fluoride) (pVDF). pCTFE and chlorotrifluoroethylene (CTFE)/vinylidene fluoride (VDF) copolymers are frequently used industrially as films. pVDF is used as a piezoelectric material. pCTFE and pVDF are both highly crystalline materials. pVDF has been intensely studied because of its interesting crystalline phases and piezoelectric properties. There has been less work, however, on the melt phase of pVDF. pCTFE is an unusually dense, highly crystalline polymer. There have been several experimental studies of CTFE/VDF[3−5] copolymers, mostly focusing on systems with low VDF content. The random CTFE/VDF copolymers at room temperature are much less crystalline than the homopolymers, while maintaining the high densities characteristic of the homopolymers. Relatively little is known regarding the structural features of these polymeric systems in the melt. Moggi et al.[4] have studied the CTFE/VDF copolymers of varying degrees of crystallinities, over a wide composition range, and have found that the structural characteristics, as obtained from wide-angle X-ray scattering (WAXS) measurements, were virtually unvaried in the copolymers up to CTFE/VDF ≈ 75 mol %.

In the past decade or so, molecular dynamics (MD) simulations have been used extensively to study the equilibrium and dynamic properties of many polymeric materials.[6−22] Less attention, however, has been given to polymers containing fluorine.[20−22] This is partly because of difficulties in simulating systems with Coulombic interactions. Increases in computational resources and the development of reliable force fields[17−19,23] have made it feasible to include Coulombic interactions in polymer simulations. Copolymers have also been given less attention than the corresponding homopolymers.

In this paper we examine structural features of several random copolymers of CTFE and VDF. We focus particular attention on a copolymer with an approximate 3:1 mole ratio of CTFE to VDF. This material is known as Kel-F 800. Kel-F 800 finds practical use as a binding agent in the manufacture of high explosives. The high density, chemical stability, and high compressibility of Kel-F 800 make it particularly useful in this application.[24]

We employ molecular dynamics simulations and wide-angle X-ray scattering to understand the structure of CTFE/VDF copolymers and homopolymers. The MD results presented here also show a similar structural shift at CTFE/VDF ≈ 75 mol %, as mentioned above. We attempt to explain the underlying cause of this observation. Additionally, we are interested in the relationship between the copolymer composition and the long-ranged Coulombic interactions. To this end, we study several features of the polymer structure, including radial distribution functions, characteristic ratios, and torsional angle distributions. We also examine the interpretation of WAXS when applied to halopolymers.

* To whom correspondence should be addressed.

10.1021/ma001077a CCC: $20.00
Published on Web 03/30/2001

We find that the WAXS spectrum is complicated by many underlying element pair scattering contributions.

II. Computational Method

A. Polymer Representation. The following CTFE/VDF copolymers were simulated: 100, 72, 50, 25, 15, and 0 mol % CTFE. The amorphous bulk copolymer microstructures consisted of a single chain composed of 120 monomer units; simulations were performed using periodic boundary conditions. All the atoms in the polymer chain were treated explicitly. The use of single chain polymers to represent bulk amorphous melts and glasses is common and has proven to be quite accurate in replicating the behavior of experimental polymeric systems.[8−12,15,16,21,15] To validate the use of a single chain to represent amorphous polymer structures, we performed simulations of nine oligomeric pCTFE and random 3:1 (Kel-F 800) copolymer chains, each consisting of 19 monomer units per chain. The multichain and single-chain systems gave identical thermodynamic and structural results to within statistical simulation errors.

We generated the initial starting homopolymer/copolymer configurations with a Monte Carlo algorithm.[26] Either a CTFE or VDF monomer was randomly added to the growing copolymer chain with a probability proportional to the product of the monomer concentration and the monomer reactivity ratio. The reactivity ratios for the CTFE and VDF monomers were chosen to be $r_1 = 0.75$ and $r_2 = 0.73$, respectively, based on the reactivity data reported by Moggi et al.[4]

Head-to-tail reversal probabilities were chosen to be in accord with those found for the corresponding homopolymers.[4,27] A head-to-tail reversal probability of 2% was used for CTFE, while a reversal probability of 5% was used for VDF. In Kel-F 800 simulations, the 120-monomer unit chain had one CTFE reversal and two VDF reversals. To test the effects of the random chain sequence in the Kel-F 800 polymer chain, including differing the number of monomeric reversals, on the structural properties to be presented, simulations were undertaken at a single temperature (450 K) for several different chain sequences (including the multichain system described above). It was found that the changes in the polymer chain sequence gave nearly identical structural and thermodynamic results (see section IV).

All other compositions, including the pCTFE homopolymer, were simulated without any reversals. All polymers were isotactic. The initial atomic positions of the amorphous melt structure were generated using a random distribution of torsional angles. The resulting amorphous structure was then relaxed by energy minimization.

B. Potential Functions. The COMPASS force field parameter set (version 98.02)[23,28] was used throughout. COMPASS was developed to improve upon existing force fields for use in simulating polymers and organic molecules. The COMPASS force field are the same as the CFF-type force fields,[28] which may be divided into two categories: valence terms, which include cross-coupling terms, and nonbonded terms. The valence terms consist of bond, angle, torsion, and out-of-plane angle terms. The cross terms include bond−bond, bond−angle, bond−torsion, bend−bend, and angle−angle−torsions. The nonbonded interactions are of the Lennard-Jones 9−6 potential type for the van der Waals terms and a Coulombic function for an electrostatic interaction. The electrostatics consist of partial charges on each atomic species and are derived from ab initio calculations. All valence degrees of freedom were explicitly treated and unconstrained. Nonbonded interactions were truncated for atom pairs with an interatomic distance greater than 9.5 Å (where the approximate cell dimension of the simulated systems were ∼20−23 Å). The truncation was implemented using a fifth-order spline between 8.5 and 9.5 Å to avoid discontinuities in the energies at the cutoff. A buffer width of 0.5 Å was used in the generation of the neighbor list. Charge groups were defined to avoid the introduction of artificially produced monopoles due to the cutoff, where each monomer unit is defined as a charge group. The nonbonded neighbor list thus included all atoms assigned to the given charge group if any atom in the group was within the cutoff range.

C. Molecular Dynamics Method. The amorphous polymer structures were simulated using three-dimensional cubic periodic boundary conditions. The Verlet velocity[29] time integration method was used with a time step of 0.5 fs. All simulations employed constant particle number, N, pressure, and temperature (NPT) dynamics at an average pressure of 0 atm. The Andersen[30] method was used for the temperature and pressure control in the constant NPT dynamics.

All initial configurations were generated with a bulk melt density of 1.0 g/cm^3. The low initial density, as compared to the approximate experimental melt densities of −2.0 g/cm^3 at 300 K for Kel-F 800, was found to improve the convergence of the equilibration procedure by avoiding high-energy initial configurations. Each system was initially simulated at 550 K. In all simulations, the periodic box was allowed to relax under NPT conditions. Equilibration at this temperature was carried out for at least 1 ns for all copolymers.

For pCTFE and Kel-F 800, simulations were performed at 10 different temperatures: 550, 500, 450, 400, 350, 300, 225, 200, 150, and 50 K. Equilibration at each temperature was carried out for a minimum of 1 ns for Kel-F 800, while equilibration of pCTFE was carried out for a minimum of 5 ns because of the slower relaxation times observed in the pCTFE simulations. For temperatures in the melt phase (300−550 K) a constant average volume was achieved during equilibration. The pressure, temperature, potential energy, Coulombic energy, van der Waals energy, and total energy also achieved constant averages.

Data collection for Kel-F 800 at temperatures above 300 K took place for a minimum of 1 ns. Data for pCTFE above 300 K were collected for up to 5 ns. For temperatures below 300 K, a longer data collection phase of up to 10 ns was employed for both polymers. Below 300 K complete equilibration was not found on the simulation time scale. In this case only the final state was used to generate $V-T$ properties.

The other CTFE/VDF copolymers compositions were simulated at temperatures of 550 and 450 K. At each temperature equilibration consisted of a NPT MD simulation for a minimum of 2.5 ns. Data collection then occurred for a period of between 2.4 and 2.9 ns in NPT MD simulations. pVDF was simulated at temperatures of 550, 500, and 450 K. At each temperature both equilibration and data collection occurred for 5 ns under NPT in MD runs.

All computations were carried out with the DISCOVER molecular dynamics program.[26] The computations were performed on Silicon Graphics Octane R12000 workstations.

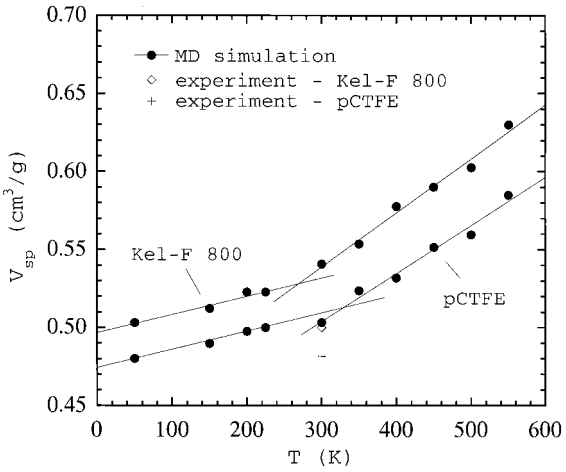

Figure 1. Specific volume vs temperature for pCTFE and Kel-F 800 at 0 atm as determined from *NPT* dynamics. The MD simulations results and experimental values are both shown.

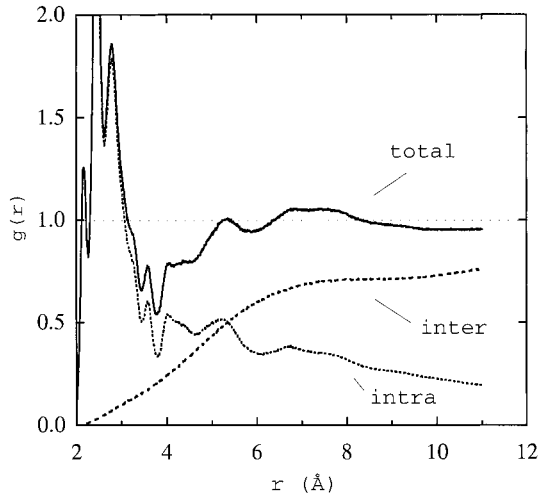

Figure 2. Radial distribution function for Kel-F 800 at 450 K. The total $g(r)$ (solid line) is decomposed into intermolecular, $g^{inter}(r)$, (dashed line) and intramolecular, $g^{intra}(r)$, (dotted line) contributions.

III. Experimental Section

Samples of amorphous Kel-F 800 (3-M Co., $M_w = 57\,000$, $T_g \approx 30$ °C) were prepared by heating the samples to 120 °C for 30 min, pressing at 500 psi to the desired thickness, and cooling at 18 °C/min. Differential scanning calorimetry showed no melt transition in the region from 60 to 120 °C. WAXS data were collected with the Advanced Polymer Beamline at the National Synchrotron Light Source at Brookhaven National Laboratory. The samples were heated in a beamline furnace, and measurements were made in transmission. A 1-D position-sensitive detector was used to collect data for 2θ angles between 8° and 36°; angle calibration was against polyethylene standards.

IV. Results and Discussion

A. Volume−Temperature Results. The calculated specific volumes for pCTFE and Kel-F 800 as a function of temperature are shown in Figure 1. The volume vs temperature curves for both pCTFE and Kel-F 800 show a distinct break characteristic of vitrification.[7−14] The extraction of the volumetric T_g in this manner is common, albeit only empirically justified.[7−14] The calculated volumetric T_g in Figure 1 is seen to be ∼290 K for Kel-F 800 and ∼325 K for pCTFE. The T_g values compare well with the experiment, 295−307 K[24] for Kel-F 800 and ∼325 K for pCTFE.[5] The calculated specific volume of Kel-F 800 at 300 K is 0.54 cm^3 g^{-1} compared to an experimental value of 0.50 cm^3 g^{-1}.[31] The calculated specific volume of pCTFE is 0.50 cm^3 g^{-1} compared to an experimental result for fully amorphous pCTFE of 0.48 cm^3 g^{-1}.[32]

The discrepancies in both the specific volume and T_g for Kel-F 800 are arguably consistent. Since the calculated density is too low, we expect an overprediction of the molecular mobility, and thus a T_g that is somewhat lower than the experimental range. The agreement here, however, is reasonable, since no attempts were made to calibrate the potential energy parameters.

The calculated volumetric coefficient of thermal expansion, $\beta = V_0^{-1}[\partial V/\partial T]_p$, above T_g is found to be ∼6.4 × 10^{-4} °C^{-1} for Kel-F 800 and ∼6.1 × 10^{-4} °C^{-1} for pCTFE at 300 K, where $[\partial V/\partial T]_p$ was extracted using a linear least-squares fit and V_0 is the reference volume at 300 K. The linear coefficient of thermal expansion (LCTE) for both Kel-F 800 and pCTFE is $^1/_3$ of β (∼2 × 10^{-4} °C^{-1}), since the system is isotropic. The calculated LCTE is roughly consistent with the earlier range of values reported for Kel-F 800 by Cady and Caley[24] of (3−16) × 10^{-4} °C^{-1} and pCTFE[33] of 2.5 × 10^{-4} °C^{-1} above T_g.

B. Radial Distribution Functions for Kel-F 800. We first examine structural aspects of bulk amorphous melts of CTFE/VDF copolymers using radial distribution functions,[34] $g(r)$. It is desirable to distinguish between intramolecular and intermolecular contributions to the radial distribution function [i.e., $g(r) = g^{inter}(r) + g^{intra}(r)$]. We decomposed the single long chain in periodic space into effective inter- and intramolecular contributions by first "unwrapping" the periodic box chain coordinates into a continuous chain. If the distance between two atoms in unwrapped coordinates was equal to the distance of the closest periodic image, the atom pair was assigned to $g^{intra}(r)$. Otherwise, it was assigned to $g^{inter}(r)$.[35]

Figure 2 shows the total, intermolecular, and intramolecular radial distribution functions for Kel-F 800 at 450 K. The relatively close contacts between nonbonded atoms are caused by the soft Lennard-Jones 9−6 potential used in the force field. Figure 2 also shows that the intermolecular radial distribution function shows little structure.

In Figure 3, the intermolecular radial distribution function is further decomposed into elemental radial distribution functions:

$$g^{inter}(r) = \frac{1}{N(N-1)} \sum_{i \le j}^{N} g_{ij}^{inter}(r) \qquad (1)$$

where the sum occurs over the N element types. In contrast to $g^{inter}(r)$, the elemental radial distribution functions show distinct structure, with first maxima ranging from 3.5 to 6.8 Å. An estimate of the first neighbor interchain spacing can be determined from the CC radial distribution function, which has a maximum at 6.9 Å. Features that begin to appear at a distance of half the cell length suggest a second neighbor spacing beginning to emerge. To evaluate the emergence of the second neighbor peak, simulations were performed on a Kel-F 800 melt twice the size as that discussed previously (see section IIA). In these simulations second

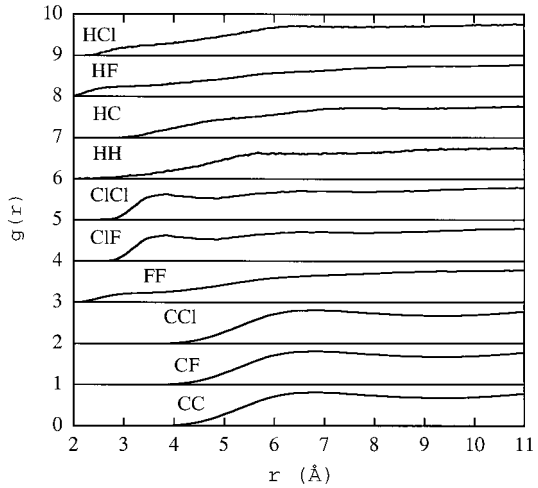

Figure 3. Kel-F 800 atom−atom radial distribution functions $g_{ij}^{\text{inter}}(r)$ are shown at 450 K. The curves have been shifted for clarity.

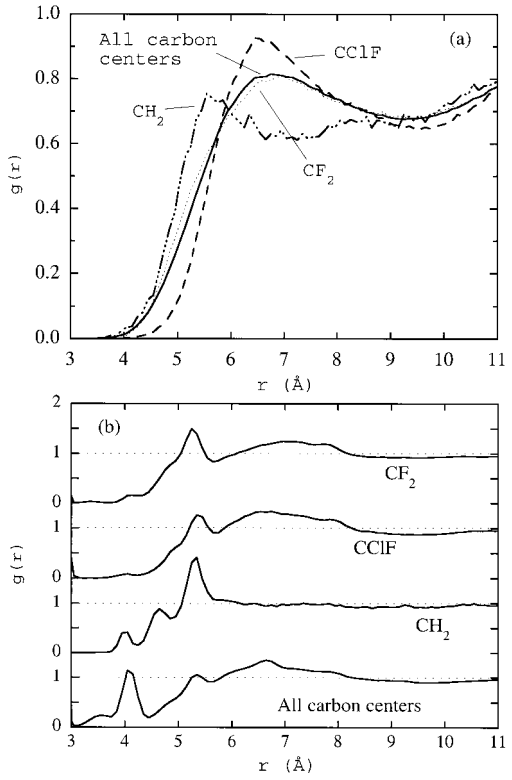

Figure 4. Kel-F 800 carbon based site−site radial distribution function at 450 K. The site−site radial distribution functions shown are for all main-chain carbon atoms, carbons with pendent fluorines (CF_2), carbons with pendent hydrogens (CH_2), and carbons with pendent fluorine and chlorine (CClF) atoms. Panel a represents the intermolecular site−site radial distribution functions; panel b represents the total site−site radial distribution functions. The curves have been shifted for clarity. Lines are labeled in the figure.

neighbor peak becomes discernible at ∼14.0 Å, and a third neighbor peak is also evident at around 21.0 Å.

The interchain spacing is made clear in Figure 4. This figure shows further decomposition of the main-chain carbon atom radial distribution function into site−site inter- and intramolecular radial distribution functions based on the functional group. For example, $g_{CF_2-CF_2}(r)$ is the radial distribution function between carbons with two pendent fluorine atoms. $g_{CH_2-CH_2}(r)$ and $g_{CClF-CClF}(r)$ are defined similarly. This distribution function may be further decomposed into intermolecular and intramolecular contributions, as discussed above. The intermolecular contributions are displayed in Figure 4a. The multiple peak positions found in Figure 4a contribute to the width of the first neighbor interchain spacing peak in $g_{CC}(r)$. The interchain spacing associated with CH_2 is smaller than that of carbons with pendant halogen atoms, because of the small size of the hydrogen atoms. The $g_{CClF-CClF}^{\text{inter}}(r)$ peak is sharper than that of $g_{CF_2-CF_2}^{\text{inter}}(r)$. We note that the CF_2 moiety occurs in both the CTFE and VDF comonomers, whereas the CClF moiety occurs only in the CTFE monomer. This makes it plausible that the distribution of CF_2-CF_2 chain distances is broader than the corresponding CClF−CClF distribution.

The contributions of the different main-chain carbon moieties to the total radial distribution function are shown in Figure 4b. Each carbon moiety total distribution function has a maximum at a shorter distance than the corresponding interchain spacing found in panel a. These peaks are obviously associated with intermolecular interactions. $g_{CH_2-CH_2}(r)$ shows additional peaks within the range 4.5−5.0 Å. Since only VDF contains hydrogen, $g_{CH_2-CH_2}(r)$ is a probe of the correlation between VDF monomers. The three-peaked structure found in $g_{CH_2-CH_2}(r)$ is attributed to correlations in which CH_2 centers are separated by either two or three intervening main-chain carbon atoms, i.e., 1−4 and 1−5 interactions, respectively, where the 1−4 interactions occur because of explicit inclusion of VDF monomeric reversals incorporated in the chain sequence of the polymer.

C. Radial Distribution Functions as a Function of Composition. We next turn our attention to the effects of the monomer concentrations on the interchain packing in the melt. $g_{C-C}^{\text{inter}}(r)$ at 450 K is shown in Figure 5. CTFE/VDF copolymers with 100, 75, and 50 mol % CTFE are shown in Figure 5a, and CTFE/VDF copolymers with 25, 15, and 0 mol % CTFE are shown in Figure 5b. In all cases the polymers were in the amorphous melt phase at 450 K. The $g^{\text{inter}}(r)$ shows a marked shift in the first neighbor interchain packing peak to smaller radial distances as the CTFE monomer concentration decreases to 25 mol % CTFE. This suggests that there is a rapid but continuous transition from interchain packing found in pCTFE to packing found in pVDF at roughly 70 mol % CTFE. This effective packing transition found at CTFE/VDF ≈ 75 mol % is consistent with the Moggi et al. X-ray scattering experiments.[4]

Figure 6 shows the position of the first maximum in the radial distribution functions $g_{CC}^{\text{inter}}(r)$, $g_{CF_2-CF_2}^{\text{inter}}(r)$, and $g_{CH_2-CH_2}^{\text{inter}}(r)$ found in Figure 5a. The peak of $g_{CC}^{\text{inter}}(r)$ gradually moves to larger distances as the CTFE content is increased. The interchain packing distance is insensitive to the CTFE content above roughly 70 mol %. The CH_2 interchain distance is insensitive to CTFE content throughout the full composition range. Consequently, the CH_2 unit is relatively insensitive to the CClF content. $g_{CF_2-CF_2}^{\text{inter}}(r)$ is more sensitive to CTFE content. The most rapid change in the peak of this function occurs between 25 and 50 mol % CTFE. Above 50 mol % CTFE the spacing remains almost constant. This suggests that the larger CClF groups dominate the interchain spacing of neighboring CF_2 groups for high concentrations of CTFE.

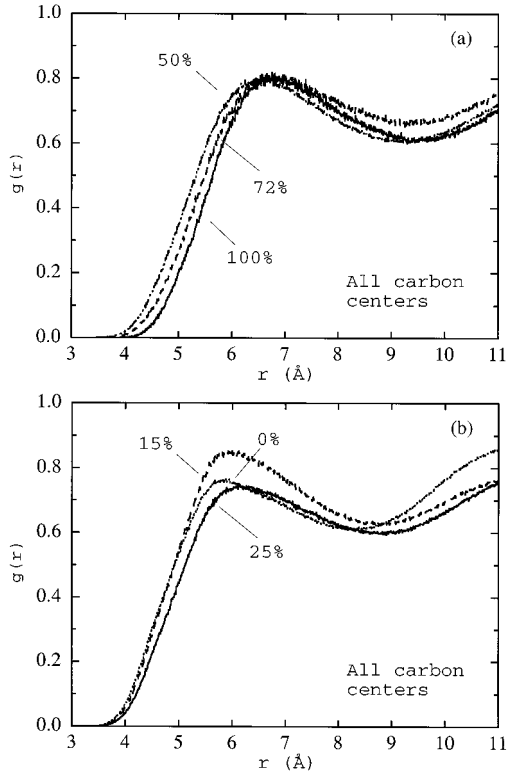

Figure 5. Intermolecular site−site main-chain carbon atom radial distribution function vs comonomer concentration at 450 K. Curves are labeled by the mole percents of CTFE. Panel a represents 100, 72, and 50 mol % CTFE; panel b represents 25, 15, and 0 mol % CTFE. Lines are labeled in the figure.

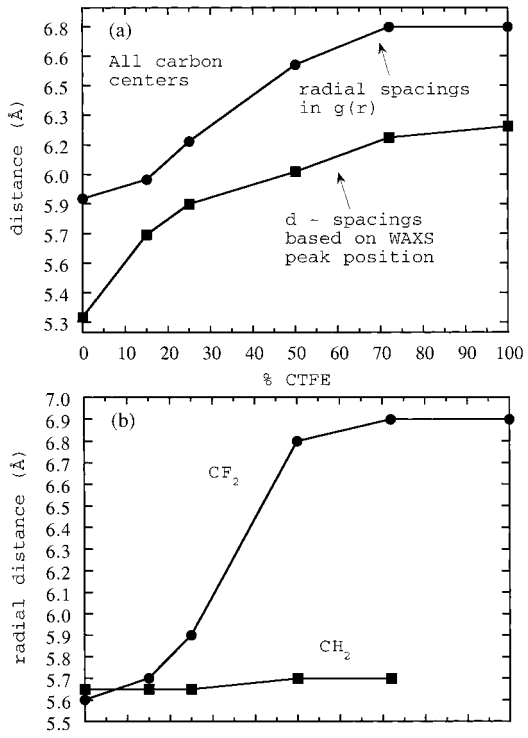

Figure 6. Intermolecular radial distribution peak positions vs % CTFE at 450 K. Panel a represents the peak positions for all carbon atoms; panel b represents peak positions for the CF_2 and CH_2 groups in the polymer chain. The solid line through the curves are to guide the eye.

D. Coulombic Interactions. The role of Coulombic interactions in determining the structure of halogenated polymers is of interest.[36,37] To that end, simulations of Kel-F 800 in the melt were performed with all the atomic charges set to zero. Figure 7 shows the total radial distribution function $g(r)$ with and without Coulombic interactions at 550 K. The distribution functions are only slightly different, with the greatest differences in the vicinity of 4−6 Å. Studies by Smith et al.[37] on poly(vinyl chloride) melts show similar insensitivity. The structural similarities seen between Coulombic and *non*-Coulombic chains are consistent with the dominant role that hard interactions play in determining the structure of simple fluids.[34]

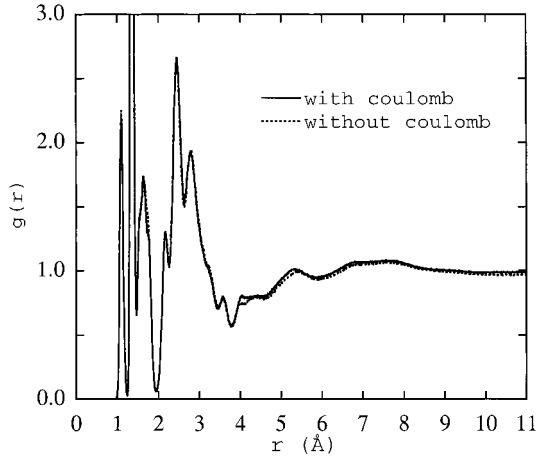

Figure 7. Radial distribution function for Kel-F 800 melts with Coulombic interactions (solid curve) and without Coulombic interactions (dotted curve) at 550 K.

E. X-ray Scattering. X-ray scattering is an important experimental probe of polymeric structures. As described in section III, WAXS experiments were performed on Kel-F 800. We present preliminary experimental results and compare them to simulation results here. For this reason, we take up discussion of the X-ray results for Kel-F 800 copolymer composition first.

The WAXS experiment measures intensity as a function of scattering vector, k. This can be obtained from simulations via Fourier transforms of $g(r)$,[38−40] using

$$I(k) = \sum_i \sum_j \left[x_i \delta_{ij} + x_i x_j \rho \int_0^\infty 4\pi r_{ij}^2 f_i(k)\, f_j(k)\, h_{ij}(r_{ij}) \frac{\sin(kr_{ij})}{kr_{ij}}\, \mathrm{d}r_{ij} \right] \quad (2)$$

where r_{ij} is the radial distance between atom i and atom j, ρ is the total average density, and $h_{ij}(r_{ij}) = g_{ij}(r_{ij}) - 1$ is the total radial distribution function between atoms of elemental types i and elemental type j. x_i and $f_i(k)$ are the number fraction and atomic scattering factor of the i-type atom. The radial distribution functions, $g_{ij}(r_{ij})$, were determined in MD runs. The scattering factors were taken from Cullity.[39]

Figure 8 compares the X-ray scattering profile computed from simulation results at 450 K with experimental results for Kel-F 800 at 473 K in the melt. The X-ray scattering data are plotted as a function of the scattering angle 2θ, where $k = 4\pi \sin\theta/\lambda$ and λ is the wavelength of the X-rays, 1.307 Å for the data displayed here. Three peaks centered at Bragg spacings, $d = \lambda/2 \sin\theta$, of 6.2, 2.5, and 1.3 Å are present in the simulation results, corresponding roughly to interchain, intrachain second neighbor, and intrachain first neighbor dis-

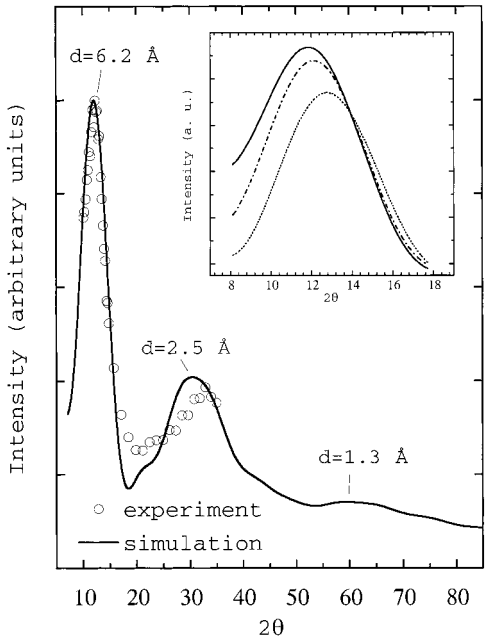

Figure 8. X-ray scattering intensity vs scattering angle at 450 K as obtained from simulation (solid line). Experimental results are at 473 K (open circles). The X-ray wavelength is 1.307 Å. The inset shows the calculated X-ray scattering intensity for various temperatures: $T = 550$ K (solid line), $T = 450$ K (dash−dotted line), and $T = 300$ K (dotted line).

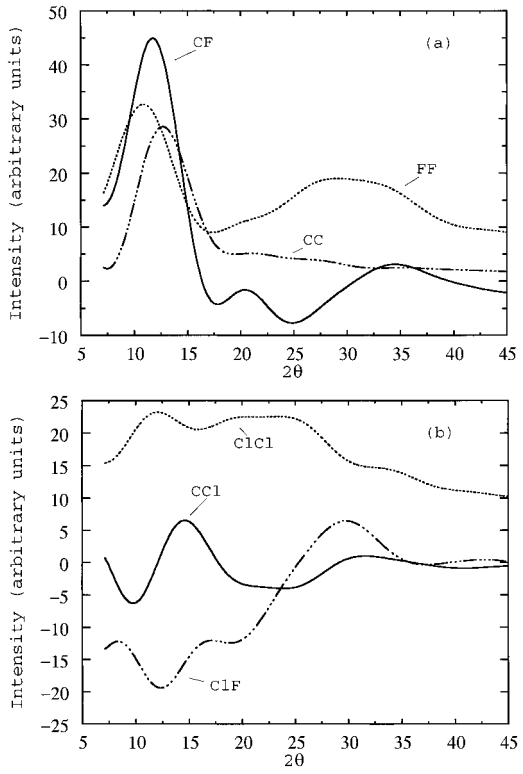

Figure 9. Calculated Kel-F 800 atom−atom X-ray scattering intensities. The hydrogen contributions have been removed for clarity. Lines are labeled in the figure. Panels a and b contain the scattering contributions to the total scattering intensity, as shown in Figure 8.

tances. There is excellent agreement between the calculated and experimental X-ray scattering profiles over the limited range of the experiment. Best agreement is found for the first peak, which is in the range of interchain distances.

The X-ray scattering profiles for Kel-F 800 in the melt determined from simulation as a function of temperature are presented in Figure 8 (see inset). The interchain peak shifts to lower angle with increasing temperature because of thermal expansion. Note also that this peak broadens and decreases in intensity as the temperature is increased, as is expected for isotropic thermal expansion.

We next illustrate the specific contributions of each atomic species in Kel-F 800 to the total scattering intensity. Figure 9 shows each of the six atom−atom scattering intensities (CC, CF, CCl, ClCl, ClF, FF) calculated from simulation. The H scattering contributes little to the total X-ray scattering intensity and has therefore been removed for the purpose of clarity. CF scattering is the largest contribution to the intermolecular peak. The fact that CF scattering is dominant can be rationalized on the basis of the relative abundance and scattering intensity of the elements in eq 2. The CC and FF scattering, however, also contribute substantially. The wide range of peak maxima found for the major contributors is responsible for much of the width of the peak in this region.

Negative intensities are found for some unlike element pairs; these are caused by destructive interference. The total scattering due to any element pair is the sum of the diagonal (e.g., ClCl and FF) and off-diagonal (e.g., ClF) contributions, which is always found to be positive.

The intramolecular peak at $2\theta \approx 30°$ is produced mainly from the FF and ClF interactions. The width of the intramolecular peak is caused by atom−atom interactions with maxima that occur at widely varying scattering angles. Interestingly, the CC atom−atom interaction contributes very little to the overall intensity of the intramolecular peaks. This is explained by the fact that the carbon atom scattering factor, $f_C(k)$, decreases more rapidly with increasing k than either the fluorine $[f_F(k)]$ or chlorine $[f_{Cl}(k)]$ atom scattering factors.

The X-ray scattering intensities are shown as a function of comonomer concentration at 450 K in Figure 10. The interchain peak is seen at ≈12.1° for the pCTFE homopolymer and Kel-F 800 copolymer. The peak shifts to larger scattering angles as the concentration of CTFE is decreased. This is consistent with the radial distance shifts seen in Figure 6, as well the experimental X-ray results of Moggi et al.[4] However, a more dramatic shift is seen to take place when the CTFE concentration approaches zero (pVDF) in Figure 10. This is not reflected in the *all*-carbon center radial distribution functions in Figure 5 but rather more closely follows the trend seen in the packing associated with the CF_2 moiety (Figure 6b). In fact, the location of the peaks found in the X-ray data never coincide with those found from the interchain spacing peaks obtained from the *all*-carbon center radial distribution functions.

The reduction in intensity as the CTFE content decreases is produced by a decrease in the total number of fluorine atoms contributing to the total scattering intensity. The total X-ray scattering intensities for 15 mol % CTFE copolymer and pVDF deconvoluted into corresponding atom−atom contributions are shown in Figures 11 and 12, respectively. CF scattering is found to be the dominant contribution for Kel-F 800 (see Figure 9) and 15 mol % CTFE. The CC scattering intensity is relatively insensitive to composition, whereas the CF scattering intensity shows significant changes.

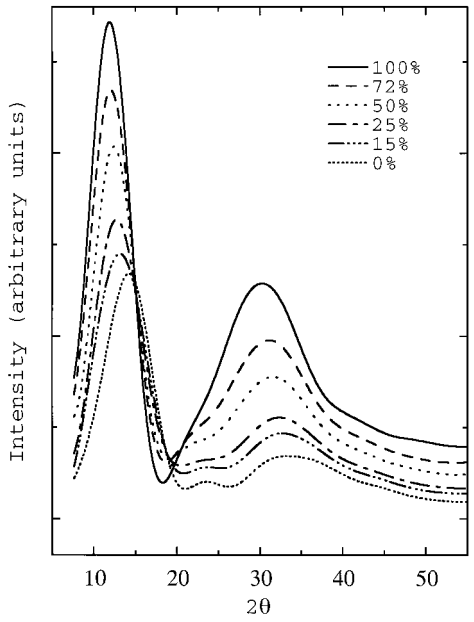

Figure 10. X-ray scattering intensities of CTFE/VDF copolymers at 450 K. Lines are labeled in the figure.

For pVDF CC scattering is larger than CF scattering. In fact, we find that the locations of the CC and total scattering peaks agree to within 0.1 Å for pVDF. The decrease in the CF scattering is also responsible for the shift in the total scattering intensity to larger angles with decreasing CTFE content.

F. Chain Conformation. Another molecular feature of interest is the characteristic ratio, C_∞. This is given as

$$C_\infty = \lim_{n\to\infty} C_n$$

$$C_n = \frac{\langle R^2 \rangle}{nl^2} \qquad (3)$$

where $\langle R^2 \rangle$ is the mean-square end-to-end distance, n is the number of main-chain (skeletal) bonds, and l is their length.[41] In the simulation, interchain distances that are greater than half the box size (∼12 Å here) are not reliable due to artifacts introduced by the periodic boundary conditions.[11]

C_n was computed by determining R^2 for each atomic pair separation more than six atoms along the polymer backbone. Previous simulations[10,11,37] have shown that extrapolation of C_n yields fairly accurate values of C_∞. The convergence of the above algorithm was determined by calculating C_∞ for two portions of a single trajectory. The results usually varied by less than 0.1, with a maximum difference of 0.2. In Table 1 we compare our calculated characteristic ratios to those of other common polymers. The computed characteristic ratios for pCTFE and Kel-F 800 are found to be very similar, indicating that end-to-end distances are insensitive to the 25 mol % VDF content. The computed C_∞ for pVDF homopolymer is found to be in excellent agreement with experiment.[42] The characteristic ratios of pCTFE and all other CTFE/VDF copolymers are found to be fairly similar to polyethylene (PE). This indicates that the presence of the halo atoms in pCTFE and other copolymers has little overall influence on chain end-to-end distances. pVDF is an exception and displays a lower value of C_∞. This is consistent with the strong shift in the first X-ray scattering peak in Figure 10.

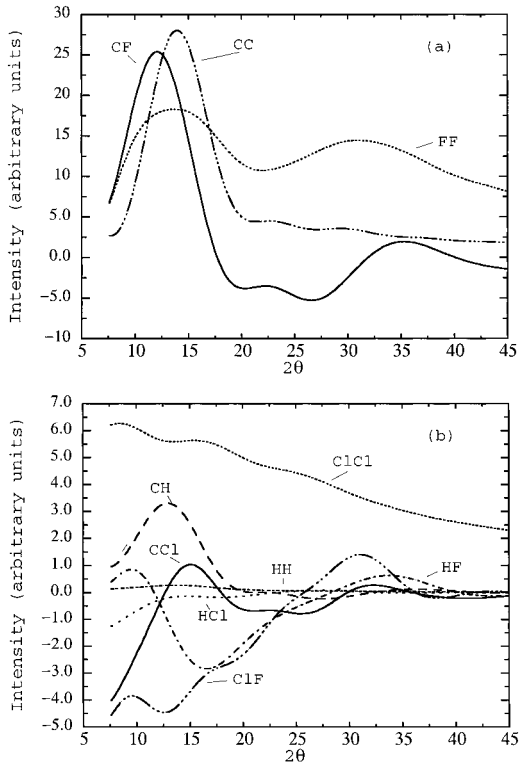

Figure 11. Calculated atom−atom X-ray scattering intensities for 15 mol % CTFE copolymer at 450 K. Lines are labeled in the figure. For clarity, individual atom−atom contributions have been separated into panels a and b.

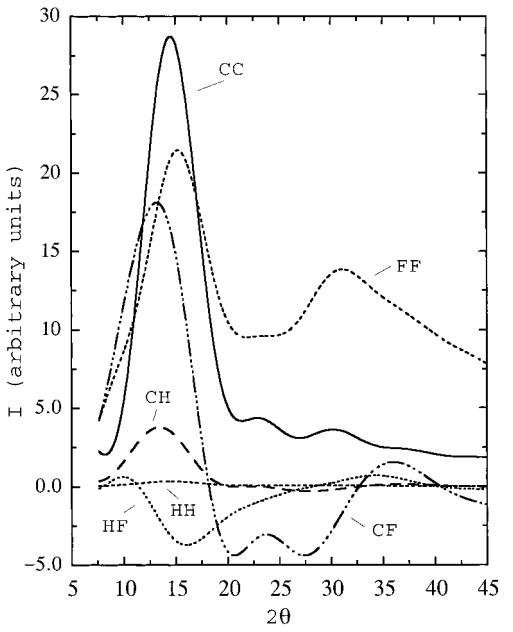

Figure 12. Calculated atom−atom X-ray scattering intensities for pVDF homopolymer at 450 K. Lines are labeled in the figure.

Perhaps one reason for the sudden shift in C_∞, seen in the pVDF homopolymer, is that the randomly placed CTFE comonomer acts to disrupt the long-ranged dipole−dipole interactions that are prevalent in the pVDF homopolymer. To test this hypothesis, C_∞ was calculated for uncharged Kel-F 800 at 550 K and uncharged pVDF at 450 K. The uncharged Kel-F 800 and pVDF melts were less dense than their charged

Table 1. Characteristic Ratio, C_∞, for Common Polymers

polymer	temp (K)	C_∞
pCTFE	450	7.1[a]
Kel-F 800 without Coulomb	550	7.7[a]
Kel-F 800	550	7.2[a]
Kel-F 800	450	7.2[a]
Kel-F 800	298	7.1[a]
50 mol % CTFE	450	6.7[a]
25 mol % CTFE	450	6.4[a]
15 mol % CTFE	450	6.3[a]
pVDF without Coulomb	450	7.7[a]
pVDF	450	5.5[a]
pVDF	463	5.6 ± 0.3,[b] 5.96[c]
poly(tetrafluoroethylene)	600	8 ± 2.5[d]
poly(vinyl chloride)	298	13.0,[e] 8 ± 1[f]
poly(vinyl chloride)	423	9.8[g]
poly(vinylidene chloride)	298	8 ± 1[h]
PE	413	6.7[i]

[a] MD results presented here. [b] Reference 42 (experimental). [c] Reference 17 (calculated). [d] Reference 43 (experimental). [e] Reference 44 (experimental). [f] Reference 45 (experimental). [g] Reference 46 (experimental). [h] Reference 47 (experimental). [i] From a tabulation by Flory in ref 41 (experimental).

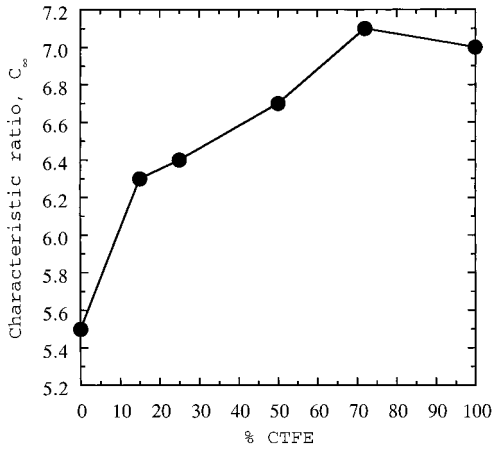

Figure 13. Calculated characteristic ratio as a function of CTFE concentration at 450 K. The solid line through the curves are to guide the eye.

analogues ($\rho_{w/}^{Kel-F800} = 1.59$, $\rho_{w/o}^{Kel-F800} = 1.52$, $\rho_{w/}^{pVDF} = 1.49$, $\rho_{w/o}^{pVDF} = 1.25$). The characteristic ratios were also greater for the uncharged polymers than the charged polymers (see Table 1). Thus, the uncharged microstructures are more extended than the charged polymers. The effects of Coulombic interactions are significantly greater for pVDF than for Kel-F 800. Also, the effect of Coulombic interactions was proportionally greater for C_∞ than for the density, indicating that polymer conformation is more sensitive to long-range interactions than packing. In Figure 14a we show the distribution of C−C−C−C torsional angles for Kel-F 800 at 300 and 550 K. A split in the trans population around 180° is observed at 300 K, which is common for fluoropolymers.[17,19,20,48] The split in the trans population first becomes apparent at 500 K and becomes more pronounced as the temperature is lowered. The asymmetry of the split seen in this region is a consequence of the asymmetric carbon with its pendant fluorine and chlorine atoms and the tacticity of the polymer (more evidence of this to be shown in Figure 15). At temperatures below the simulated glass transition temperature, T_g, a split population in the region of the gauche minima between 30° and 120° is seen. While splitting in this region is seen in similar fluoropolymers,[19,20,48] the validity of these data is questionable because of the

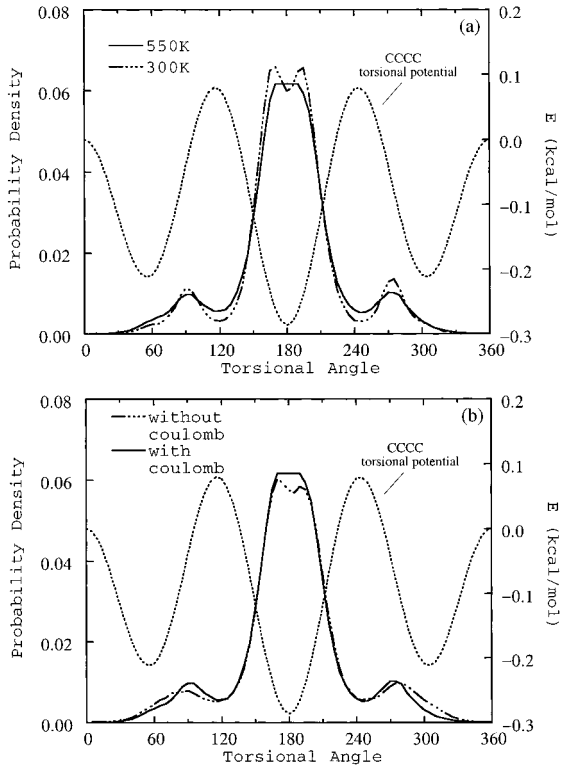

Figure 14. Calculated distribution of torsional angles. Panel a represents *fully* charged Kel-F 800 at temperatures of 550 K (solid line) and 300 K (dashed line). In panel b torsional angle distributions for charged (solid line) and uncharged (dotted line) Kel-F 800 at 550 K are compared. The CCCC torsional potential has been superimposed in each panel.

slow relaxation of torsional angles for temperatures under T_g.[8]

In Figure 14b we show the torsional distribution function at 550 K for simulations of Kel-F 800 with and without Coulombic interactions. A split trans configuration is now seen at 550 K for the *non*-Coulombic polymer. This is presumably caused by Coulombic stabilization of the energy surface in the neighborhood of 180° torsional angle.

The fully charged polymer has a greater population of torsional angles found at angles between 180° and ±15° as compared to its *non*-Coulombic analogue. However, the total trans fractions, defined as those torsional angles found between 120° and 240°, of the uncharged and fully charged polymer are found to be comparable, 0.803 vs 0.818, respectively.

The split behavior found in the distribution of C−C−C−C torsional angles, as seen in Figure 15, continues to CTFE concentrations up to 25 mol % CTFE, after which the split found in the trans state is no longer apparent. A rapid change in interchain packing (see section IVB) is seen at the same concentration.

V. Conclusion

In this paper we have undertaken a detailed examination of the structure of CTFE/VDF random copolymers and homopolymers in the melt phase. Our simulations were generally in good agreement with experiment. The $V-T$ curve at zero pressure was in acceptable agreement with experiment, including the location of the volumetric T_g. New experimental data for the WAXS spectrum of Kel-F 800 were presented here. We were able to reproduce that data. The interchain packing

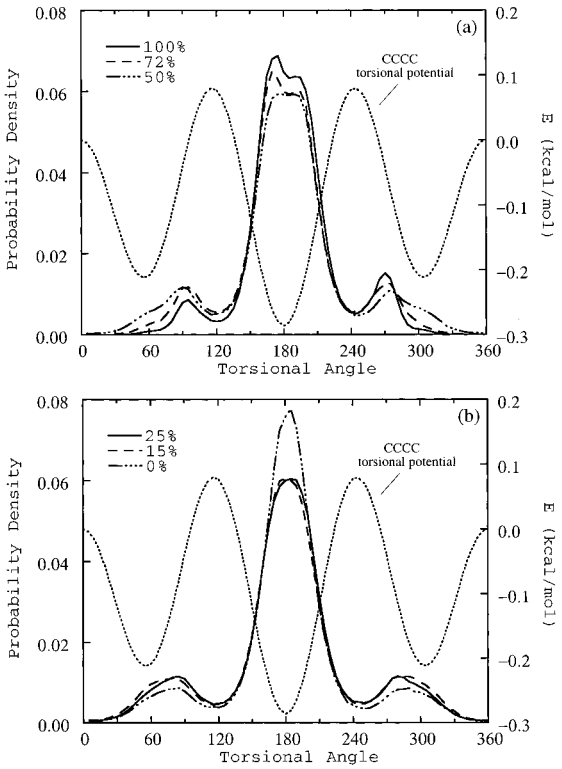

Figure 15. Calculated distribution of torsional angles as a function of CTFE concentration at 450 K. Panel a represents CTFE concentrations of 100, 72, and 50 mol %; panel b represents CTFE concentrations of 25, 15, and 0 mol %. The CCCC torsional potential has been superimposed in each panel.

dependence on the copolymer composition and the approximate mole fraction at which the transition in the interchain spacing from that seen in pCTFE to that found in pVDF are also found to be in excellent agreement with experiment by Moggi and co-workers.[4] The calculated characteristic ratios also agree well with experiment for pVDF. We conclude that the COMPASS force field accurately predicts many properties of fluoropolymers.

We found that a division of the radial distribution function into elemental, intramolecular, and intermolecular components is useful in interpreting the structure of the polymers studied here. In particular, we found that the interchain spacing is sensitive to the substituent atoms. The interchain spacing between CF_2 carbon centers can be up to 1.2 Å greater than the interchain spacing between CH_2 carbon centers.

We discovered that the interchain spacing depended strongly on the CTFE/VDF fraction. As might be expected, chain spacing increased as more bulky Cl atoms were added to the polymer. We found, however, that this increase in chain spacing did not occur uniformly throughout the chain. Instead, the CH_2 spacing remained almost constant as a function of CTFE concentration at 450 K. The CF_2 spacing, however, showed a rapid increase between 25 and 50 mol % CTFE.

We have studied the way that polymer structure is reflected in the WAXS spectrum. We found that the decomposition of the WAXS spectrum into elemental contributions to be useful in understanding the atomistic origin of the experimental spectrum. The first peak of the WAXS spectrum did not accurately represent the true C−C interchain spacing, due to C−F scattering. Our conclusion is that the WAXS spectra of halogenated polymers must be interpreted with care. The decomposition techniques employed here could be of use in interpreting the WAXS spectra of other more complicated polymers.

Halogenated polymers, unlike hydrocarbon polymers, have bulky and highly charged substituent atoms. We have examined the role that charge plays in determining the structure of CTFE/VDF copolymers and homopolymers. The total radial distribution for Kel-F 800 showed only a small dependency on Coulombic interactions. This sensitivity increased, however, as the VDF content increased. This suggests that polymer structure is more sensitive to Coulombic interactions when the monomer unit has a strong dipole moment, such as VDF. The overall chain conformation as measured by the characteristic ratio was more sensitive to Coulombic interactions than the density.

In conclusion, this work has elucidated some of the structural features of homopolymers and copolymers containing halogen atoms. Further work along these lines should help in the transition from polymer modeling based on a handful of simple model systems to the consideration of more complicated and realistic polymers and copolymers. Such a transition should be of particular benefit in the industrial application of atomistic polymer simulation techniques. Future work will focus on the interfacial structure of Kel-F 800 in high explosive composites as well as the dynamic aspects of CTFE/VDF copolymers.

Acknowledgment. The authors are pleased to acknowledge the assistance of Dr. Cheng Saw, LLNL, and Dr. Fengji Yeh, BNL, in obtaining the experimental WAXS data. This work was performed under the auspices of the U.S. Department of Energy by the University of California Lawrence Livermore National Laboratory under Contract W-7405-Eng-48.

References and Notes

(1) *Polymer Handbook*; Brandup, J., Immergut, E. M., Eds.; Wiley: New York, 1989. *Developments in Crystalline Polymers;* Lovinger, A., Ed.; Applied Sciences: London, 1981; Vol. 1.
(2) James, E. *The Development of Plastic Bonded Explosives*; UCRL-12439-T; Lawrence Livermore National Laboratory: Livermore, CA, 1965.
(3) Ramachandra, P.; Ramani, R.; Ramgopal, G.; Shariff, G.; Thimmegowda, M. C.; Sathyanarayana, P. M.; Ranganathaiah, C. *Polymer* **1999**, *40*, 5961.
(4) Moggi, G.; Bonardelli, P.; Bart, J. C. *J. Polym. Sci.* **1984**, *22*, 357.
(5) Ramachandra, P.; Ramani, R.; Ravichandran, T. S. G.; Ramgopal, G.; Gopal, S.; Ranganathaiah, C.; Murthy, N. S. *Polymer* **1996**, *37*, 3233.
(6) Takeuchi, H.; Roe, R. J. *J. Chem. Phys.* **1991**, *94*, 7446. Rigby, D.; Roe, R. J. In *Computer Simulation of Polymers*; Roe, R. J., Ed.; Prentice Hall: Englewood Cliffs, NJ, 1991; pp 79−93. Mansfield, K. F.; Theodorou, D. N. *Macromolecules* **1991**, *24*, 6283.
(7) Rigby, D.; Roe, R. J. *J. Chem. Phys.* **1987**, *87*, 7285. Rigby, D.; Roe, R. J. *J. Chem. Phys.* **1988**, *89*, 5280. Rigby, D.; Roe, R. J. *Macromolecules* **1989**, *22*, 2259. Rigby, D.; Roe, R. J. *Macromolecules* **1990**, *23*, 5312.
(8) Gee, R. H.; Boyd, R. H. *J. Chem. Phys.* **1994**, *101*, 8028. Boyd, R. H.; Gee, R. H.; Han J.; Jin Y. *J. Chem. Phys.* **1994**, *101*, 788.
(9) Pant, P. V. K.; Han J.; Smith, G. D.; Boyd, R. H. *J. Chem. Phys.* **1993**, *99*, 597. Han, J.; Boyd, R. H. *Macromolecules* **1994**, *27*, 5365.
(10) Gee, R. H.; Boyd, R. H. *Polymer* **1995**, *36*, 1435.

(11) Han, J.; Boyd, R. H. *Polymer* **1996**, *37*, 1797.
(12) Han, J.; Gee R. H.; Boyd, R. H. *Macromolecules* **1994**, *27*, 7781.
(13) Boyd, R. H. *Trends Polym. Sci.* **1996**, *4*, 12.
(14) Bharadwaj, R. K.; Berry, R. J.; Farmer, B. L. *Polymer* **2000**, *41*, 7209.
(15) Sylvester, M. F.; Yip, S.; Argon, A. S. In *Computer Simulation of Polymers*; Roe, R. J., Ed.; Prentice Hall: Englewood Cliffs, NJ, 1991; pp 105−121.
(16) *Atomistic Modeling of Physical properties of Polymers*; Monnerie, L., Suter, U., Eds.; Springer: Berlin, 1994.
(17) Byutner, O. G.; Smith, G. D. *Macromolecules*, in press.
(18) Byutner, O. G.; Smith, G. D. *Macromolecules* **1999**, *32*, 8376.
(19) Smith, G. D.; Jaffe, R. L.; Yoon, Do Y. *Macromolecules* **1994**, *27*, 3166.
(20) Holt, D. B.; Farmer, B. L. *Polymer* **1999**, *40*, 4667.
(21) Karasawa, N.; Goddard, W. A. *Macromolecules* **1995**, *28*, 6765.
(22) Karasawa, N.; Goddard, W. A. *Macromolecules* **1992**, *25*, 7268.
(23) Sun, H. *J. Phys. Chem. B* **1998**, *102*, 7338.
(24) Cady, W. E.; Caley, L. E. *Properties of Kel-F 800 Polymer*; UCRL-52301; Lawrence Livermore National Laboratory: Livermore, CA, 1977.
(25) Hedenqvist, M. S.; Bharadwaj, R.; Boyd, R. H. *Macromolecules* **1998**, *31*, 1556. Meier, R. J.; Struik, L. C. E. *Polymer* **1998**, *39*, 31.
(26) Molecular Simulations, Inc., is a provider of molecular modeling simulation software with headquarters in San Diego, CA. All simulations were done using the CERIUS^2 DISCOVER molecular dynamics program, version 4.0.
(27) Odian, G. *Principles of Polymerization*; John Wiley: New York, 1991; p 204.
(28) Hwang, M.-J.; Stockfisch, T. P.; Hagler, A. T. *J. Am. Chem. Soc.* **1994**, *116*, 2515. Maple, J. A.; Hwang, M.-J.; Stockfisch, T. P.; Dinur, U.; Waldman, M.; Ewig, C. S.; Hagle, A. T. *J. Comput. Chem.* **1994**, *15*, 162.
(29) Allen, M. P.; Tildesley, D. J. *Computer Simulation of Liquids*; Clarendon Press: Oxford, U.K., 1989, and references therein.
(30) Andersen, H. C. *J. Chem. Phys.* **1980**, *72*, 2384.
(31) DeTeresa, S. J. Private communication, Lawrence Livermore National Laboratory.
(32) Hoffman, J.; Weeks, J. *J. Chem. Phys.* **1962**, *37*, 1723.
(33) Hall, H. T. *J. Chem. Phys.* **1952**, *69*, 68.
(34) McQuarrie, D. A. *Statistical Mechanics*; Harper & Row: New York, 1976, and references therein.
(35) Pant, P. V. K.; Han, J.; Smith, G. D.; Boyd, R. H. *J. Chem. Phys.* **1993**, *99*, 597.
(36) Neelov, I.; Niemelä, S.; Sundholm, F. *J. Non-Cryst. Solids* **1998**, *340*, 235.
(37) Smith, G. D.; Jaffe, R. L.; Yoon, Do Y. *Macromolecules* **1993**, *26*, 298.
(38) Warren, B. E. *X-ray Diffraction*; Addison-Wesley: Reading, MA, 1969.
(39) Cullity, B. D. *Elements of X-ray Diffraction*; Addison-Wesley: Reading, MA, 1956.
(40) Pings, C. J.; Waser, J. *J. Chem. Phys.* **1968**, *48*, 3016.
(41) Flory, P. J. *Statistical Mechanics of Chain Molecules*; Interscience: New York, 1969.
(42) Welch, G. J. *Polymer* **1974**, *15*, 429.
(43) Chu, B.; Wu, C.; Buck, W. *Macromolecules* **1989**, *22*, 831.
(44) Nakajima, A.; Kato, K. *Makromol. Chem.* **1966**, *95*, 52.
(45) Mark, J. E. *J. Chem. Phys.* **1972**, *56*, 451.
(46) Sato, M.; Koshiishi, Y.; Asahina, M. *J. Polym. Sci., Polym. Lett. Ed.* **1963**, *1*, 233.
(47) Matsuo, K.; Stockmayer, W. H. *Macromolecules* **1975**, *8*, 660.
(48) Okada, O.; Oka, K.; Kuwajima, S.; Tanabe, K. *Mol. Simul.* **1999**, *1*, 325.

MA001077A